The Journal of Experimental Biology 210, 299-310
Published by The Company of Biologists 2007
doi:10.1242/jeb.02633

Quantitative analysis of tethered and free-swimming copepodid flow fields

Kimberly B. Catton[1], Donald R. Webster[1,*], Jason Brown[2] and Jeannette Yen[2]

[1]*School of Civil and Environmental Engineering, Georgia Institute of Technology, Atlanta, GA 30332-0355, USA and* [2]*School of Biology, Georgia Institute of Technology, Atlanta, GA 30332-0230, USA*

*Author for correspondence (e-mail: dwebster@ce.gatech.edu)

Accepted 7 November 2006

Summary

We quantified the flow field generated by tethered and free-swimming *Euchaeta antarctica* using the particle image velocimetry (PIV) technique. The streamlines around the free-swimming specimens were generally parallel to the body axis, whereas the streamlines around all of the tethered copepodids demonstrated increased curvature. Differences noted in the streamline pattern, and hence the vorticity, dissipation rate and strain rate fields, are explained by considering the forces on the free-swimming specimen compared to the tethered specimen. Viscous flow theory demonstrates that the force on the fluid due to the presence of the tether irrevocably modifies the flow field in a manner that is consistent with the measurements. Hence, analysis of the flow field and all associated calculations differ for tethered *versus* free-swimming conditions. Consideration of the flow field of the free-swimming predatory copepodid shows the intensity of the biologically generated flow and the extent of the mechanoreceptive signal quantified in terms of shear strain rate. The area in the dorso-ventral view surrounded by the 0.5 s^{-1} contour of e_{xy}, which is a likely threshold to induce an escape response, is 11 times the area of the exoskeletal form for the free-swimming case. Thus, mechanoreceptive predators will perceive a more spatially extended signal than the body size.

Key words: copepod, *Euchaeta antarctica*, hydrodynamics, tethering, sensory systems.

Introduction

One of the critical aspects of understanding the interaction between aquatic organisms and their surrounding fluid environment is the accurate quantification of flow fields created during feeding and locomotion. For instance, properly quantifying the flow field facilitates calculating the external forces created by animal propulsion (e.g. Drucker and Lauder, 2002), the energetic costs of feeding and locomotion (e.g. Stamhuis et al., 2002), and the flow disturbance created by organism motion (e.g. Yen and Fields, 1992). Flow fields generated by copepods are of particular interest because of the ecological significance of the interaction with other organisms. The flow field around a copepod is a complex structure comprising an anterior feeding current and a lateral and ventral propulsive current (Fields and Yen, 1993). A strong anterior feeding current can maximize intake volume to the feeding appendages, as might be needed by a particle feeding plankter. It follows that accurate estimates of volume processed in the feeding current are useful to assess feeding rates and ultimately the impact of copepod grazing on trophic energy transfer in planktonic communities. Alternatively, a predatory copepod may construct a feeding current with a weaker velocity gradient so as not to reveal its presence to rheotactic prey (Yen and Strickler, 1996). Thus, crypsis of the predator from its prey may be an important mechanism in determining predation success. When generating the propulsive current, trimming of the wake can be useful when hiding from mechanoreceptive predators [e.g. fish (Coombs et al., 1988)] or when creating a minimally disturbed trail of the pheromone needed to attract a mate (Yen et al., 1998).

Because of the interest in visualizing and quantifying the flow fields created by copepods, several methods have been employed in recent decades: Schlieren optics (Strickler, 1977), high-speed micro-cinematography (Alcaraz et al., 1980; Koehl and Strickler, 1981; Strickler, 1982; Gallager, 1993), manual particle tracking (Yen et al., 1991; Yen and Fields, 1992; Fields and Yen, 1993; Bundy and Paffenhöfer, 1996), planar particle image velocimetry (PIV) (van Duren et al., 1998; van Duren et al., 2003; Stamhuis et al., 2002; van Duren and Videler, 2003), and three-dimensional digital holography (Malkiel et al., 2003). Because copepods are (generally) small, visualization of the flow field created by copepods requires high resolution. As a result, copepods are often tethered in order to maintain a fixed position within the small field of view during flow visualization. In the majority of the studies listed above, the copepod was tethered during the flow visualization process. Researchers generally acknowledge the distortion of the flow field induced by tethering the organism but tethering is often

considered a necessary step for acquiring flow field data. For instance, during PIV measurements the copepod and surrounding fluid must be imaged when the body position coincides with a thin laser sheet. In absence of tethering, the researcher may have to wait patiently for the organism to swim through the imaging region of the laser sheet and hope that the body orientation is ideal during the pass. Obviously, this is a potentially tedious experimental procedure. As an alternative, researchers have suggested adding a fixed translational velocity to the measurements around tethered copepods to account for the differences in the flow field (e.g. Koehl and Strickler, 1981). It also has been suggested that placing a tethered copepod in a moving current (at a speed that matches a typical swim velocity) eliminates the potential influence of the tether on the flow field (Bundy and Paffenhöfer, 1996).

Despite the common use of tethering of zooplankton during flow studies, a comparison between untethered and tethered larvae showed that the flow pattern is altered by the presence of the tether (Emlet, 1990). Further, the magnitude and location of high velocity regions are different in tethered *versus* untethered copepods and larvae (Emlet, 1990; Bundy and Paffenhöfer, 1996). In addition to the physical differences in the flow field, the organism behavior is also potentially modified by the addition of the tether. Hwang et al. found similar mean time allocation habits of tethered copepods compared to untethered copepods (Hwang et al., 1993), but there was a significant difference in the individual variability.

The objective of this study was to quantitatively compare the flow fields created by tethered and untethered copepodids using the particle image velocimetry (PIV) technique. As described in detail below, the fields of velocity, vorticity, dissipation rate and strain rate created by the copepodid *Euchaeta antarctica* were quantified for free-swimming and tethered specimens. Because events occur at time scales of milliseconds for organisms in the millimeter range, the measurements require high precision in timing and high spatial resolution.

Materials and methods

Collection of organisms

Euchaeta antarctica Giesbrecht 1902 individuals were collected at Croker Passage at latitude 64°05′S and longitude 62°50′W in the Southern Ocean during November 2003. The collected specimens were juvenile CV copepodids with a prosome length of 4.6 mm. Copepodids were sorted into 2 liter containers of chilled seawater and hand-carried to our laboratory at the Georgia Institute of Technology in Atlanta, Georgia, USA. In the laboratory, the specimens were placed in a dark environmental chamber at 0°C. The copepodids swam freely in 19 liter buckets with gentle aeration and were fed phytoplankton and brine shrimp nauplii. All measurements were performed within the first month since capture, although the copepodids lived for over 3 months in the laboratory.

Experimental setup

Flow fields created by free-swimming and tethered *E. antarctica* were visualized in a clear, glass cubic tank (15 cm×15 cm×15 cm) filled with artificial seawater of salinity 34.85 p.p.t. in a dark room. The temperature of the tank was maintained at 0°C during the experiment by immersing the glass tank in a recirculating bath of propylene glycol and deionized water, which was surrounded by insulating foam with small windows to provide optical access for the cameras. The recirculating bath fluid passed through a Fisher Scientific chiller in order to maintain the desired temperature. Images of free-swimming copepodids were recorded only when the copepodids swam through the laser sheet. A second camera, connected to a television monitor and possessing a perspective perpendicular to the PIV camera, was used to monitor the position of the free-swimming copepodids.

To restrain the copepodid, we tethered it to a 38-gauge copper wire attached by cyanoacrylate glue. Attachments were made to the dorsal side of the copepodid near the junction between the cephalic and thoracic segments. A 0.5 mm bend at the end of the wire provided enough surface area for attachment. The end of the wire, dipped in glue and air-dried for 30 s until the glue was tacky, was attached to a copepodid, which was restrained in a drop of water in a cooled Petri dish. Just prior to attachment, the copepodid was blotted dry of seawater for less than 1 s. Once the tacky end of the wire made contact with the dorsal side of the copepodid, ambient seawater was added to harden the glue and ensure attachment. The copepodid was fully submerged in seawater, and the copepodid–wire bond was checked for proper attachment and positioning away from the cephalic appendages. Copepodids with a poorly positioned tether were not used for flow field imaging. The bend directed the wire away from the copepodid at a right angle to minimize interference with the deployment of the locomotory appendages, although as noted below the presence of the tether appeared to influence the symmetry of the resultant biologically generated flows. The wire was attached *via* a glass rod to a 3-axis precision position manipulator, which was used to position the copepodid in the laser sheet in the center of the field of view of the camera.

Fluid velocity measurements

Flow fields were measured for free-swimming and tethered *Euchaeta antarctica* using the non-intrusive particle image velocimetry (PIV) technique. The PIV technique measures the displacement of small tracer particles suspended in the fluid over a short time period (e.g. Westerweel, 1997; Raffel et al., 1998). The advantage of this technique is that the position of many particles can be recorded with a digital camera; hence, a field of simultaneous velocity vectors is measured. Because the particles were illuminated by a laser sheet, the displacement vectors corresponded to the plane of illumination. One important assumption for PIV is that the particles follow the fluid flow over the measurement interval; therefore, tracer particles must be small and nearly neutrally buoyant. In the current experiments, titanium dioxide particles with a mean diameter of less than 5 μm were homogeneously seeded into the fluid.

The particles were illuminated with an Oxford pulsed infrared laser (model HSI-500, Shirley, MA, USA). The laser illuminated particles in a 1 mm thick sheet with a row of laser diodes that produced monochromatic light at a wavelength of 808 nm and maximum pulse energy of 15 mJ. Many copepods are phototactic, respond to light by swimming towards it, and are typically most sensitive to wavelengths centered around 500 nm (Stearns and Forward, 1984; Cohen and Forward, 2002). The near IR wavelengths employed in the current measurements did not change the organism behavior. Specifically, the copepodids swam freely into and out of the laser sheet with no observable avoidance or preference and with no observable change in swimming characteristics. The laser pulse repetition period was variable within the range of 1–80 ms with the longer delay period corresponding to greater output energy and illumination. In this set of experiments, the period between the laser pulses was 8 ms and a timing control circuit synchronized the camera shutter with the laser pulses. A VDS Vosskühler CMC-1300 CMOS digital camera and a Datacube MaxRevolution image acquisition board acquired the images. Image pairs (i.e. images of the laser pulses separated by 8 ms) were collected at 50 Hz. The width of the laser sheet (1 mm) is relatively large compared to the size of the copepodid body (prosome length of 4.6 mm). As a result, the 'planar' velocity measurements correspond to a finite width of the three-dimensional flow. Based on the camera lens focal length (105 mm), aperture (f/2.8) and location, the depth of field was calculated to be 0.725 mm. Therefore, the reported velocity fields correspond to the average over the depth of field rather than true planar velocity fields.

Pairs of PIV images were analyzed to determine the particle displacement in the image plane *via* a cross-correlation calculation (e.g. Raffel et al., 1998). The images were divided into interrogation subwindows of 32×32 pixels. Particle locations in a subwindow in the first image were compared to the corresponding subwindow in the second image by calculating the cross-correlation function in phase space. The average particle displacement in the subwindow region was determined by locating the peak value of the cross-correlation function relative to the center of the subwindow. The location of the peak in the correlation was identified to subpixel accuracy *via* a Gaussian function fit. This process was repeated for the entire image with a 50% overlap of each subwindow. The velocity was calculated by dividing the displacement vector by the time delay between consecutive laser pulses. The velocity data were validated by calculating the median velocity of a 3×3 grid of neighboring points and comparing the local velocities to the median velocity (Westerweel, 1994; Nogueira et al., 1997). Velocity vectors outside of an acceptable range were identified as bad vectors and replaced by a spatially interpolated value. Velocity vectors that coincided with the location of the organism body were removed during post-processing by creating a blanking template from the original image pair. Based on the accuracy of the peak correlation location estimate and other considerations, the uncertainty of the velocity vector is estimated to be ±3%.

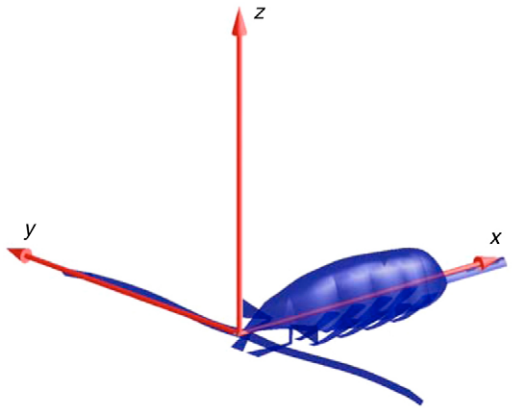

Fig. 1. Coordinate system for the flow analysis.

Flow field analysis

The coordinate system (shown in Fig. 1) for the flow field analysis was aligned with the body of the copepodid such that the origin of the coordinate system is at the head of the organism. The x direction is along the body axis, the y direction corresponds to the transverse coordinate in the dorso-ventral view (positive direction corresponding to the right side antennae), and the z direction corresponds to the transverse coordinate in the side view (positive direction corresponding to the dorsal side of the copepodid). The velocity components in the x, y and z directions are u_x, u_y and u_z, respectively. The reported velocity vectors correspond to the average value for samples collected within a 1 s period. The individual velocity fields were shifted before averaging such that the coordinate origin was always coincident with the head of the organism. The PIV data were rotated to be in the same orientation as the tethered copepodid, using the appropriate transformations for vector and tensor (e.g. strain rate) quantities.

The spatial gradient of velocity is important from a mechanosensory perspective and previous studies suggest that strain rate is the quantity that most closely correlates with copepod behavior (e.g. Fields and Yen, 1997; Kiørboe et al., 1999; Woodson et al., 2005). Strain rate is a measure of the deformation of a fluid element as it flows. The strain rate components that can be directly calculated based on the measured planar velocity fields are:

$$e_{xx} = \left(\frac{du_x}{dx}\right), \quad e_{yy} = \left(\frac{du_y}{dy}\right), \quad e_{zz} = \left(\frac{du_z}{dz}\right),$$

$$e_{xy} = \frac{1}{2}\left(\frac{du_x}{dy} + \frac{du_y}{dx}\right), \quad e_{xz} = \frac{1}{2}\left(\frac{du_z}{dx} + \frac{du_x}{dz}\right). \quad (1)$$

Vorticity $\boldsymbol{\omega}$ is another quantity based on the velocity gradient and hence also could be important to define the perturbation created by an organism, although currently there is no direct

evidence to support the idea that predators or prey are sensing and responding to vorticity. Vorticity is a point measure of the rotation of the fluid, and the components of the vorticity vector for the measured planes are:

$$\omega_z = \frac{1}{2}\left(\frac{\partial u_y}{\partial x} - \frac{\partial u_x}{\partial y}\right), \quad \omega_y = \frac{1}{2}\left(\frac{du_x}{dz} - \frac{du_z}{dx}\right). \qquad (2)$$

Another quantity involving spatial gradients of the velocity field is the viscous dissipation rate of kinetic energy. This quantity is of interest because it relates to the costs of propulsion, the time that a flow perturbation persists, and the ecological significance of predator avoidance. The rate of energy dissipation due to viscosity, Ψ, is defined as (e.g. Schlichting and Gersten, 2000):

$$\Psi = \mu\left[2\left(\frac{\partial u_x}{\partial x}\right)^2 + 2\left(\frac{\partial u_y}{\partial y}\right)^2 + 2\left(\frac{\partial u_z}{\partial z}\right)^2 + \left(\frac{\partial u_x}{\partial y} + \frac{\partial u_y}{\partial x}\right)^2 + \left(\frac{\partial u_x}{\partial z} + \frac{\partial u_z}{\partial x}\right)^2 + \left(\frac{\partial u_y}{\partial z} + \frac{\partial u_z}{\partial y}\right)^2\right]. \qquad (3)$$

Several derivative terms in Eqn 3 cannot be calculated directly from the planar PIV data. For instance, for data in the x–y plane the u_z component of velocity and derivatives in the z direction cannot be determined directly. In this case, the $\partial u_z/\partial z$ term was estimated using the incompressible continuity equation:

$$\frac{\partial u_z}{\partial z} = -\frac{\partial u_x}{\partial x} - \frac{\partial u_y}{\partial y}. \qquad (4)$$

The other unknown terms are assumed to be approximately equal to a measured term, specifically:

$$\left(\frac{du_x}{dz} + \frac{du_z}{dx}\right)^2 \approx \left(\frac{du_x}{dy} + \frac{du_y}{dx}\right)^2 \text{ and } \left(\frac{du_y}{dz} + \frac{du_z}{dy}\right)^2 \approx \left(\frac{du_x}{dy} + \frac{du_y}{dx}\right)^2. \qquad (5)$$

Therefore, the energy dissipation rate approximated in terms of the gradients calculated in the x–y plane is:

$$\Psi = \mu\left[2\left(\frac{\partial u_x}{\partial x}\right)^2 + 2\left(\frac{\partial u_y}{\partial y}\right)^2 + 2\left(\frac{\partial u_x}{\partial x} + \frac{\partial u_y}{\partial y}\right)^2 + 3\left(\frac{\partial u_x}{\partial y} + \frac{\partial u_y}{\partial x}\right)^2\right]. \qquad (6)$$

An analogous equation was employed for the x–z plane.

Results

In this experiment, PIV images of five tethered individuals and three free-swimming individuals were collected. The replicate data were qualitatively similar to the data shown in the figures and the similarities are discussed in later sections. The data shown herein were selected for publication because the animal's trajectory was centered in the image region.

Table 1. *Swimming speed and Reynolds number for Euchaeta antarctica CV copepodids based on three-dimensional trajectory observations*

Mode	Swimming speed (cm s^{-1})	Reynolds number	N
Cruising	1.46±0.62	12±5	38
Escaping	13.65±4.80	105±45	29

Values are means ± s.d. N is the number of individual specimens observed. For the cruise mode, between 11 and 120 measurements of swimming speed for each individual were collected depending on the length of the observed path. For the escape mode, between 4 and 18 measurements of swimming speed for each individual were collected.

The characteristic velocity and length scales in the Reynolds number are the swimming speed and prosome length, respectively.

To compare among free-swimming and tethered flow fields, it was important to check that the swimming behavior of the copepodids was similar. Several criteria were used to confirm that all tested specimens were behaving in a typical cruising mode. First, the raw image sequences of the free-swimming and tethered copepodids were viewed to verify that the second antennae were being used to propel the organism. The second antennae are used for propulsion during cruising, whereas the antennules (first antennae) and swimming legs are used for propulsion during escaping. Occasionally, we observed the appendage motion associated with escape behavior in both the free-swimming and tethered specimens, but the data presented herein are exclusively associated with cruise swimming behavior. Second, we confirmed that the swimming speeds of the free-swimming copepodids for the reported PIV data (0.83 cm s^{-1} for the dorso-ventral view, and 0.82 cm s^{-1} for the side view) were consistent with typical swimming speeds for cruising copepodids. Table 1 shows the average and standard deviation of the swimming speed and Reynolds number measured for a total of 67 individual specimens. Typical swimming speeds of cruising organisms are an order of magnitude smaller than the typical escaping speeds. Third, we measured the appendage paddling frequency and found that both the tethered and free-swimming copepodids were paddling at approximately 50 Hz.

Flow field

The streamlines of the flow field for the free-swimming copepodid in both the dorso-ventral and side views slightly converged in front of and slightly diverged behind the body of the organism (Fig. 2A,C). These images were created by tracking tracer particle movement in the frame of reference of the copepodid. While the streamlines around the free-swimming copepodid were nearly parallel to the body of the specimen (Fig. 2A,C), the streamlines around the tethered

copepodid curved sharply into the feeding appendages and abdomen (Fig. 2B,D). More pronounced convergence (upstream) and divergence (downstream) of the streamlines was evident for specimens in the figures and the replicates that are not shown. Qualitatively, the volume of fluid influenced by the tethered copepodid appeared to be greater than the volume of fluid influenced by the free-swimming copepodid in agreement with previous observations for larvae of bivalves and gastropods (Emlet, 1990) and for larvae of mollusks (Gallager, 1988). Specifically, Emlet noted that the particle paths were much wider upstream for the tethered specimen compared to the free-swimming organism (Emlet, 1990), which agrees with Fig. 2.

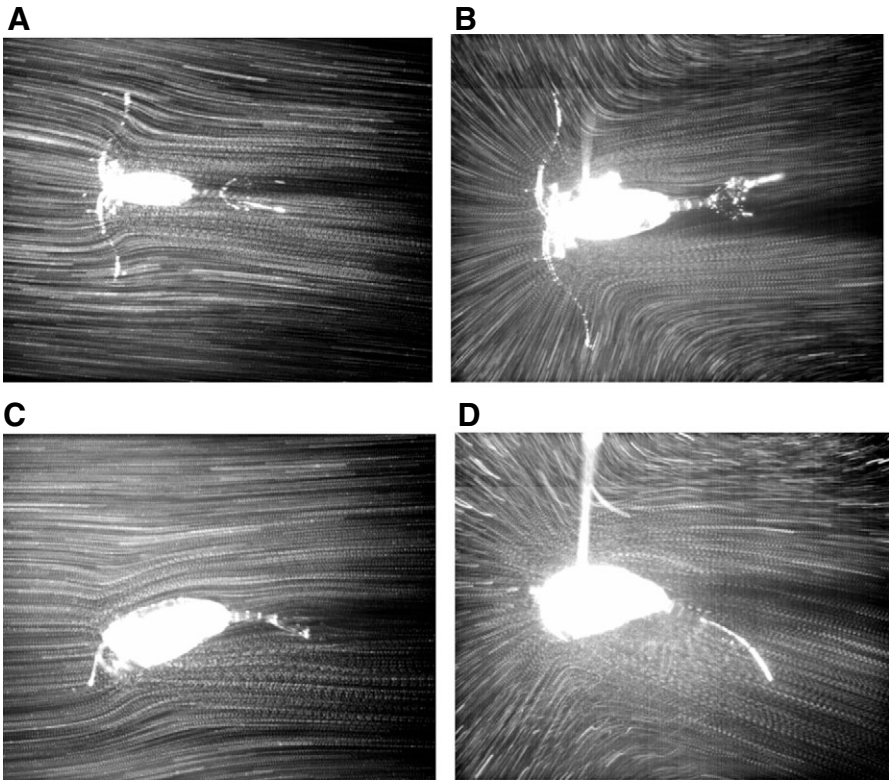

Fig. 2. (A,B) Dorso-ventral and (C,D) side views of tracer particle paths around (A,C) a free swimming and (B,D) a tethered *Euchaeta antarctica.*

Velocity field

The velocity around the body of the free-swimming copepodid was symmetrical about the line y=0 with a maximum velocity of 1.2 cm s^{-1} occurring approximately 0.05 cm to the side of the abdomen of the copepodid (Fig. 3A). The velocity vectors for the free-swimming copepodid were nearly parallel to the body of the copepodid. In contrast, the velocity around the body of the tethered copepodid was asymmetrical with maximums of 0.8 cm s^{-1} on the right side (y>0) and 1.4 cm s^{-1} on the left side (y<0) (Fig. 3B). The maximum velocities in the replicate were similarly asymmetric with maximum values of 0.3 cm s^{-1} and 0.9 cm s^{-1} on each side. For the figure and replicate fields, the larger magnitude of velocity occurred on the side of the body that was opposite to the tether connection to the position manipulator. The flow asymmetry appeared to result from the effect of the tether presence on the movement of the cephalic appendages. The tethered copepodids preferentially paddled on the side opposite of the tether in all images. The velocity vectors on the side of the copepodid facing the tether mount were directed outward from the body and the velocity vectors on the opposite side of the tether were directed into the copepodid body. In front of the copepodid, the free-swimming specimen created a low velocity region (0.2 cm s^{-1}), whereas the tethered copepodid created a higher velocity region (0.6 cm s^{-1}).

In the side view, the maximum velocity below the ventral side of the specimen (z<0), was greater for the free-swimming copepodid (maximum velocity of 1.4 cm s^{-1}) than for the tethered copepodid (maximum velocity of 1.1 cm s^{-1}) (Fig. 4). The high velocity region below the copepodid in the side view was larger in magnitude and confined to a smaller region for the free-swimming specimen.

Vorticity field

For the free-swimming copepodid, the vorticity field (Fig. 5) also demonstrated (anti)symmetry about the y=0 axis. The vorticity magnitude was largest in the boundary layer region near the body. Because of the opposite orientation of the velocity gradient, the vorticity on the left and right sides of the body had opposite signs; in both cases the maximum magnitude of the vorticity was roughly 20 s^{-1}. In the side view, the region of high vorticity magnitude also was confined to the near body boundary layer and in particular along the ventral surface of the copepodid. In this plane, the maximum vorticity magnitude also was roughly 20 s^{-1}.

Dissipation rate field

Kinetic energy was dissipated by viscous effects at relatively high levels along the sides of the free-swimming copepodid (y=0.1 cm, y=–0.1 cm), behind the antennules, along the ventral surface (z<0), and along the dorsal surface (z=0.1 cm) (Fig. 6). The maximum dissipation rate for the free-swimming copepodid occurred along the ventral surface (28 W m^{-3}). Although not shown in a figure, the peak value of dissipation rate for the tethered copepodid was similar (roughly 30 W m^{-3}). The total energy dissipation rate is calculated by integrating the dissipation rate, which is a point function, over the region of flow. Table 2 summarizes the total energy dissipation rate in the planar velocity field (W m^{-1}) by the tethered and free-

swimming copepodids. The total energy dissipation rate was larger for the tethered copepodids in all cases but the difference was greatest in the side view cases. Based on these planar data and assuming axisymmetry, a rough estimate of the total dissipation rate in the fluid volume influenced by the copepodid is around 1×10^{-8} W. This is an order of magnitude larger than the estimate for *Euchaeta rimana* (Yen et al., 1991) and two orders of magnitude larger than the estimate for *Temora longicornis* (van Duren et al., 2003). The difference may result from the fact that *E. antarctica* is larger than the other species. Further, increased resolution of the measurements may improve (and increase) the dissipation rate estimate due to better resolution of the spatial variation in velocity.

Strain rate field

The e_{xx} component of the strain rate tensor is shown in Fig. 7 for the free-swimming copepodid. As with the other quantities described above, the location of the largest values of the strain rate was in the boundary layer region near the copepodid body. The peak value was approximately 10 s^{-1} along the appendages and the ventral surface of the copepodid. A peak negative value of –10 s^{-1} occurred along the antennae in front of the copepodid (i.e. x=–0.05 cm). Other components of the strain rate tensor showed a similar spatial distribution and will be discussed below for a specific profile location.

Example profiles

The field plots are useful because they reveal spatial variability of the quantities. However, the field plots are limited in the respect that it is difficult to make definitive comparisons between the free-swimming and tethered specimens. To further examine the similarities and differences between the flow characteristics around the free-swimming and tethered copepodids, profiles of the velocity, vorticity and strain rate were extracted from the fields. Profiles are shown in Fig. 8 for flow quantities along a profile axis direction that was perpendicular to the copepodid body axis in the dorso-ventral view. To best match the spatial location of the flow field, the position of the profile was specified such that it passed through the location of the maximum in velocity magnitude for each specimen (shown in Fig. 8). Several other profile orientations were examined during this study with similar observations as the current example.

As described for the field plots in Fig. 3, the velocity direction and magnitude were altered by the presence of the tether. In Fig. 8A,B, the peak value of the u_x-component of velocity was greater in the tethered case, and the u_y-component differed in

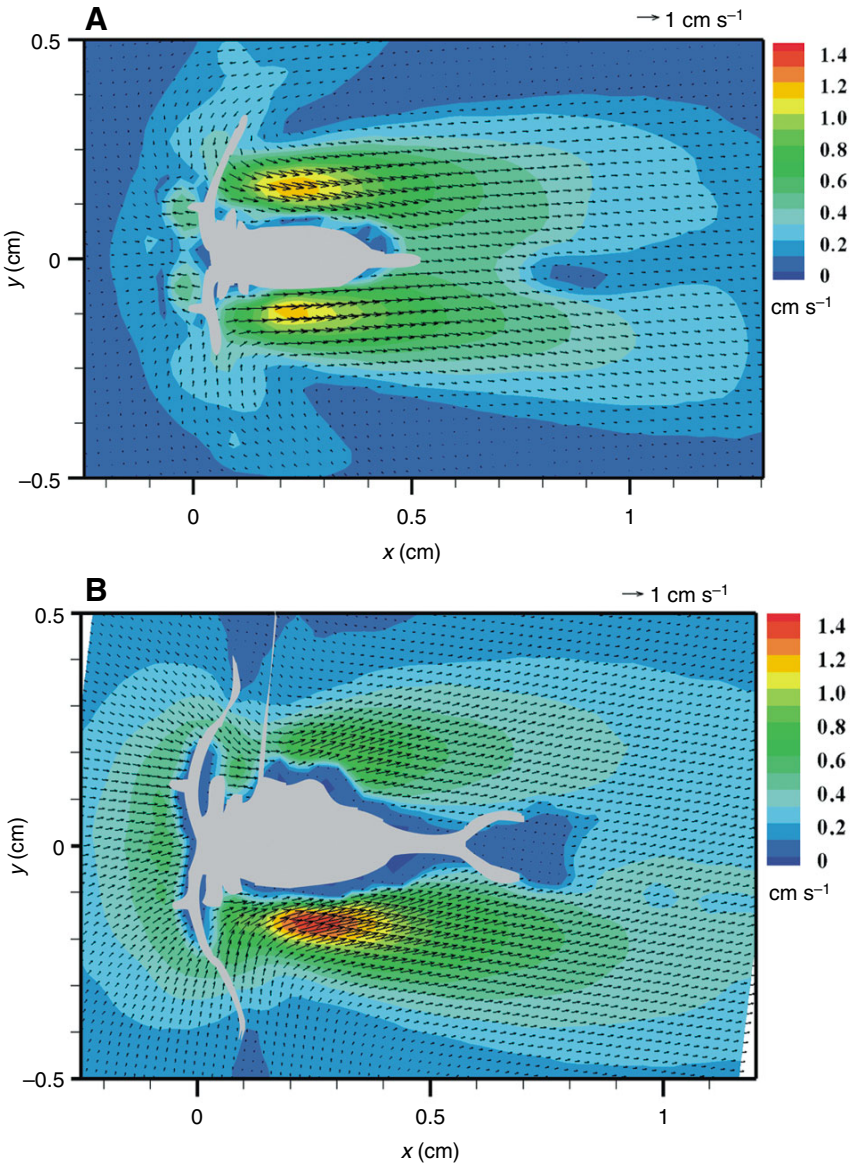

Fig. 3. Velocity vectors and contours of velocity magnitude time-averaged over one second for a (A) free-swimming, and (B) tethered *Euchaeta antarctica* for the dorso-ventral view.

Table 2. *The total energy dissipation rate of a cruising copepodid in the planar velocity field*

	Energy dissipation rate (W m^{-1})	
	Side view	Dorso-ventral view
Tethered	7.5×10^{-6} (2.1×10^{-5}, 1.1×10^{-5})	9.3×10^{-6} (8.0×10^{-6})
Free-swimming	4.7×10^{-6}	5.2×10^{-6} (7.8×10^{-6})

Replicate values are shown in parentheses.

magnitude and direction over much of the profile. The vorticity (Fig. 8C) and shear strain rate (Fig. 8F) profiles in this case agreed fairly well between the specimens, except very close to the copepodid body (y'<0.05 cm), where the magnitude of both quantities was greater in the tethered case. The normal strain rate components (shown in Fig. 8D,E) were different between the tethered and free-swimming profiles. This reflected both a change in the velocity components (Fig. 8A,B) and a change in the spatial variation (i.e. gradient) of the velocity field.

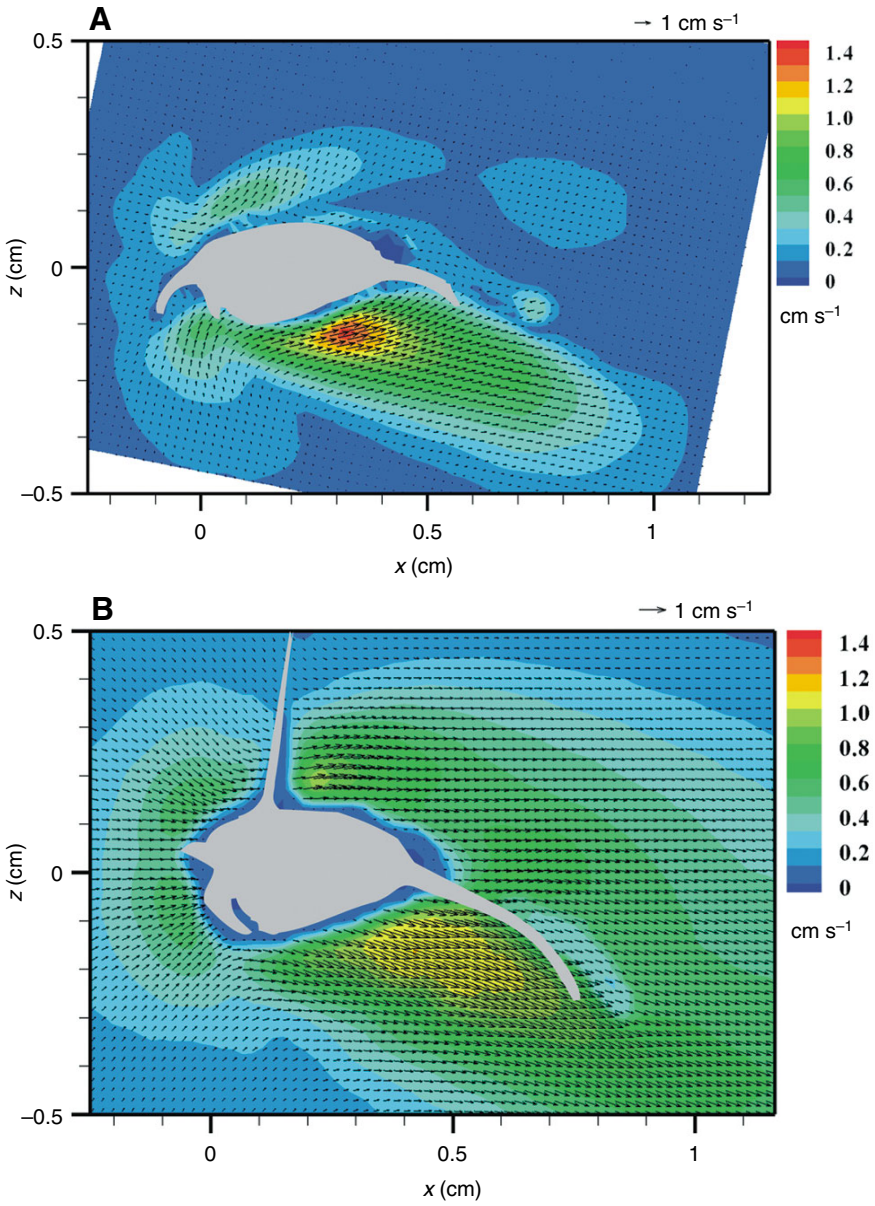

Fig. 4. Velocity vectors and contours of velocity magnitude time-averaged over one second for a (A) free-swimming, and (B) tethered *Euchaeta antarctica* for the side view.

Discussion

Effects of tethering

As presented in the Results and by other researchers (Emlet, 1990; Bundy and Paffenhöfer, 1996), the flow field around a tethered organism differs from that around a free-swimming animal. On this note, van Duren et al. write "*there is no doubt that the morphology of flow fields [around tethered copepods] will be to some extent different from those around moving animals*" (van Duren et al., 2003). At first thought, it seems intuitive to suggest that the difference is merely due to a translational velocity difference due to the fixed position of the tethered specimen compared to the moving specimen. However, the particle trajectories shown in Fig. 2 demonstrate that the difference is not solely due to the addition of a uniform velocity field corresponding to the translation of the organism. In both sets of images, the particles are moving past a copepodid fixed in the photograph, and it is clear that the particle paths are very different. Further, the data in Figs 3, 4, and 8 provide quantitative evidence that the presence of the tether greatly influences the flow field characteristics.

To explain the fundamental difference between the tethered and free-swimming flow fields, it is illuminating to consider the forces. The free body diagrams for the organism in the free-swimming and tethered cases are sketched in Fig. 9. For an organism swimming in the horizontal direction (as shown in the sketch), the relevant forces on the copepod are the drag and thrust. For an organism that is cruising, i.e. not accelerating, the forces acting on the body are in equilibrium, which means they are equal and opposite in direction. Each force acts on the organism in one orientation and on the fluid in the opposite orientation. On the organism, F_{thrust} acts in the direction of copepod motion, and F_{drag} acts opposite to the direction of copepod motion. On the fluid, F_{thrust} acts opposite to the direction of copepod motion and induces a fluid jet away from the organism, and F_{drag} acts in the direction of copepod motion and causes fluid to be dragged along with the organism.

The force balance changes meaningfully with the addition of a tether. The (non-accelerating) organism can now impart an unbalanced force on the fluid because it can push against the tether. The resistance to acceleration is not provided by a drag force, but is given rather by the force and moment on the tether. The force and moment on the tether balance F_{thrust} and act out of, and not on, the fluid (Fig. 9B). Hence, adding a translational velocity to the tethered flow field (a kinematic operation) does not take into account the force F_{drag} that results from fluid viscosity and causes fluid to be dragged along with the organism

(a dynamic effect). [Note that an equally valid description of this phenomenon has been made with regard to a 'momentumless wake' for a self-propelled object (e.g. Naudascher, 1965; Sirviente and Patel, 2000). The term 'momentumless wake' refers to the momentum distribution in the wake of the self-propelled object having the same momentum flux as the approaching flow upstream of the object. The addition of a tether alters the momentum distribution in the wake due to the addition of the unbalanced force on the fluid.]

The difference between the flow fields is largely explained by the unbalanced force in the tethered case. An analytical solution of the Navier–Stokes equations for the laminar flow induced by a point force was first reported by Landau (Landau, 1944) and Squire (Squire, 1951). The analysis begins by locating a force at the coordinate origin within an infinitely large fluid domain. The point force and polar coordinate system are shown in Fig. 10A. The solution for the flow velocity components is:

$$u_r = \frac{2\nu}{r}\left[\frac{2\cos\theta}{(C+1-\cos\theta)} - \frac{\sin^2\theta}{(C+1-\cos\theta)^2}\right], \quad (7)$$

$$u_\theta = \frac{-2\nu}{r}\frac{\sin^2\theta}{(C+1-\cos\theta)}, \quad (8)$$

and the streamfunction is:

$$\psi = 2\nu r\frac{\sin^2\theta}{(C+1-\cos\theta)}, \quad (9)$$

where C is a constant related to the strength of the force imposed at the origin (Squire, 1951):

$$\frac{F}{2\pi\rho\nu^2} = \frac{32}{3C}\frac{1+C}{2+C} + 4(1+C)^2\ln\left(\frac{C}{2+C}\right) + 8(1+C). \quad (10)$$

In these equations, r and θ are the polar coordinates, ν is the fluid kinematic viscosity, ρ is the fluid density, and F is the magnitude of the applied force. Sherman (Sherman, 1990) provided an alternative interpretation of C in which the radial velocity component, u_r, is evaluated along the downstream axis (i.e. θ=0) at an arbitrary distance r=R:

$$\frac{Ru_r\big|_{\substack{r=R\\ \theta=0}}}{\nu} = \frac{4}{C}. \quad (11)$$

Note that the left hand side appears like a local Reynolds number evaluated at r=R and θ=0. We used the measured velocity field for the tethered copepodid to estimate the velocity at a distance of 0.75 cm downstream of the tether location. The resulting value for C was 0.4.

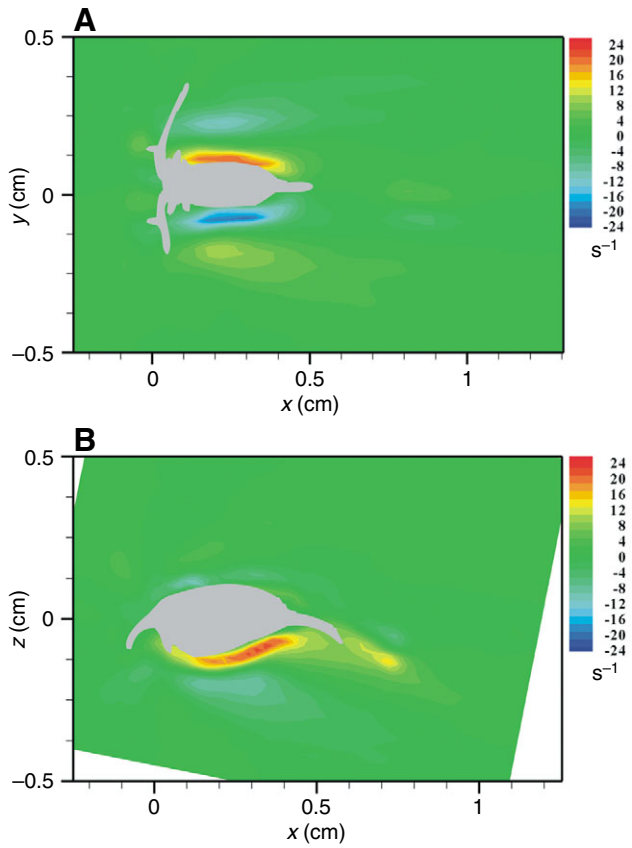

Fig. 5. Contours of the vorticity field created by a free-swimming *Euchaeta antarctica* for the (A) dorso-ventral view (ω_z), and (B) side view (ω_y).

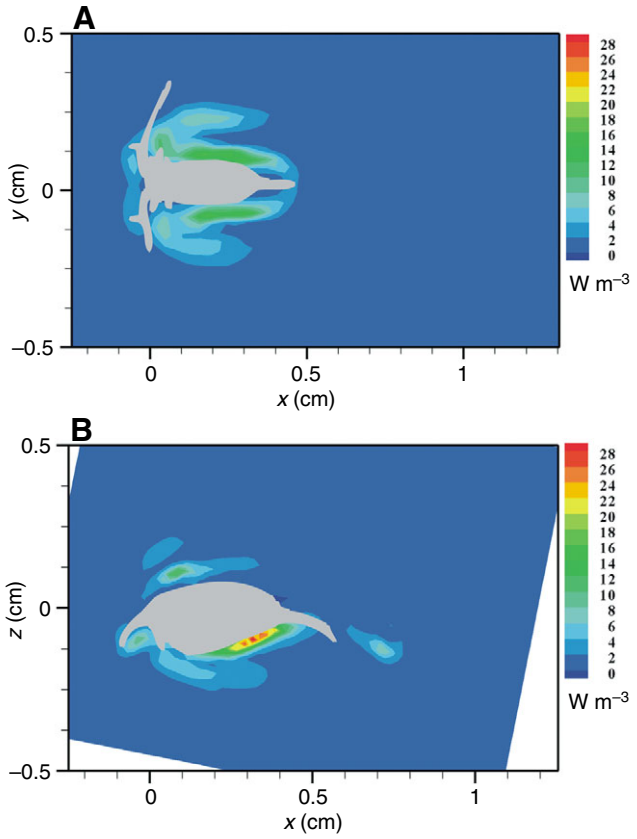

Fig. 6. Contours of dissipation rate (Ψ) for a free-swimming *Euchaeta antarctica* for the (A) dorso-ventral view, and (B) side view.

Fig. 10B shows the streamline pattern for the analytical flow solution. The streamlines converge upstream of the force location and diverge more gradually downstream. Comparison of the analytical streamline pattern with the particle paths for the tethered copepodid in Fig. 2B,D reveals a remarkable similarity. Despite the presence of the organism body and the fact that the force on the fluid is more broadly distributed in the organism case compared to the theoretical case, the general agreement suggests that the addition of a force on the fluid at the tip of the tether provides an explanation of the modified flow field for the tethered case compared to the free-swimming case.

Based on this Discussion, we can draw some important practical conclusions. The flow field in the tethered case cannot be 'corrected' by adding a uniform translational velocity (Koehl and Strickler, 1981). Rather, the addition of the unbalanced force in the tethered case modifies the flow field due to the viscous flow effects. The modified flow field has different spatial gradients and hence different fields of vorticity, strain rate and dissipation rate. Further, calculations performed during previous investigations of the filtering rate, volume of fluid entrained by zooplankton, and spatial extent of the fluid disturbance are influenced by the modification of the the flow field. One solution to this dilemma is to perform the velocity field measurements on free-swimming organisms, as done in the current study. An alternate solution is to place a tethered organism in a moving current (Bundy and Paffenhöfer, 1996), but implementing this strategy raises difficult practical issues. To eliminate the unbalanced force effect described above, the drag force due to the fluid moving past the organism body must exactly balance the self-generated thrust of the organism. The flow velocity in the test channel must be adjusted such that force on the tether equals zero, which in practical application requires that the force on the tether be measured (continuously). Because the tethered copepodid specimens demonstrate unsteady thrust generation (i.e. their swimming behavior and thrust force varies in time), data collection should be limited to periods when the measured force on the tether equals zero.

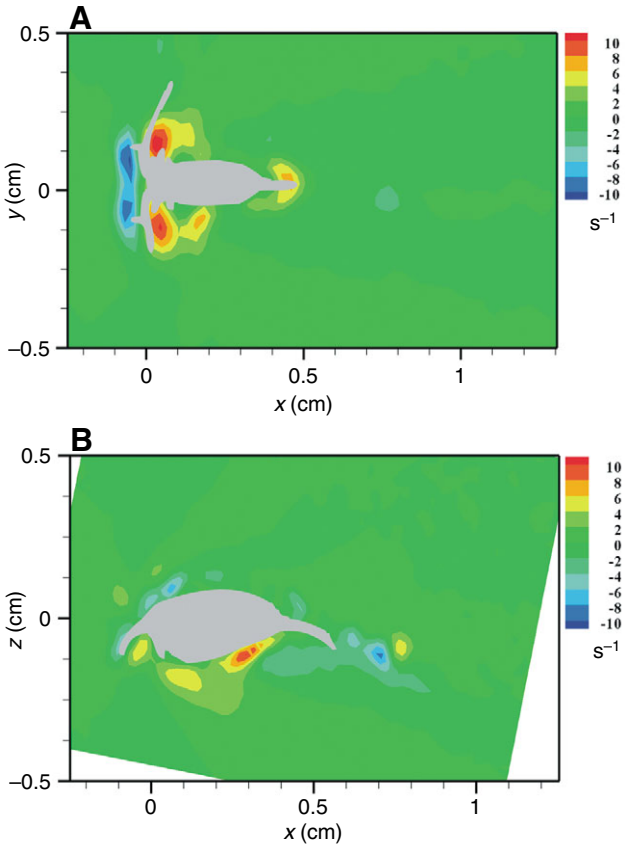

Fig. 7. Contours of strain rate (e_{xx}) for a free-swimming *Euchaeta antarctica* for the (A) dorso-ventral view, and (B) side view.

Flow field of the free-swimming copepodid

Researchers have quantified the flow fields around tethered copepods (Bundy and Paffenhöfer, 1996; van Duren et al., 1998; van Duren et al., 2003) and free-swimming copepods (Tiselius and Jonsson, 1990; Yen et al., 1991; Fields and Yen, 1993; Bundy and Paffenhöfer, 1996; Malkiel et al., 2003). The copepodids in these studies exhibited three locomotive modes: feeding, cruising and escaping. Both simulations (Jiang et al., 2002) and experiments (Tiselius and Jonsson, 1990; Bundy and Paffenhöfer, 1996) have shown that the geometry of the flow field is dependent on the locomotive mode. The current discussion is limited to the cruise mode of swimming.

Flow fields for free-swimming copepods have not been measured previously with planar PIV, but data from lower resolution particle tracking and holography methods provide useful information for comparison to the current results. In light of the discussion above regarding the modification of the flow field due to the presence of the tether, we did not make detailed comparisons to previous planar PIV data for tethered copepods despite the fact that the data in those studies have superior resolution than the particle tracking and holography methods. Malkiel et al. (Malkiel et al., 2003) observed large-scale recirculation of the fluid surrounding sinking, feeding copepods. The current data do not reveal the recirculation pattern because the data are locally focused around the organism body and the fact that the copepodids were moving in cruise mode.

Analyses of the small-scale fluid motion of the pelagic copepodid offers some insight into factors influencing the complexity of the biologically-generated flow. For this free-swimming polar species, *E. antarctica*, the magnitude of the velocity field shows a maximum (1.2 cm s^{-1}) surrounding the locomotory appendages, the second antennae. Velocity fields of free-swimming copepods have maximum velocity magnitudes ranging from 0.3 cm s^{-1} to 3.8 cm s^{-1} (Tiselius and Jonsson, 1990; Yen et al., 1991; Fields and Yen, 1993; Bundy and Paffenhöfer, 1996) and 1.98 cm s^{-1} in the simulations of Jiang et al. (Jiang et al., 1999). The velocity fields for these copepods were symmetrical in the dorso-ventral view with converging streamlines into the appendages and diverging streamlines to the rear of the organism (Tiselius and Jonsson, 1990; Yen et al., 1991). The geometry of the flow field was similar in the current study, and the maximum velocity (1.2 cm s^{-1}) was in the same

range. The velocity distribution in the current study differed from that observed by Bundy and Paffenhöfer (Bundy and Paffenhöfer, 1996), who reported considerable variability among trials. The resolution of the velocity field around the locomotory appendages is superior in the current study, which could lead to better estimates of the velocity and may explain the discrepancy. Overall, the current flow field measurements are qualitatively consistent with the previous data collected with other methods and provide improved quantitative details while avoiding the issues of tethering.

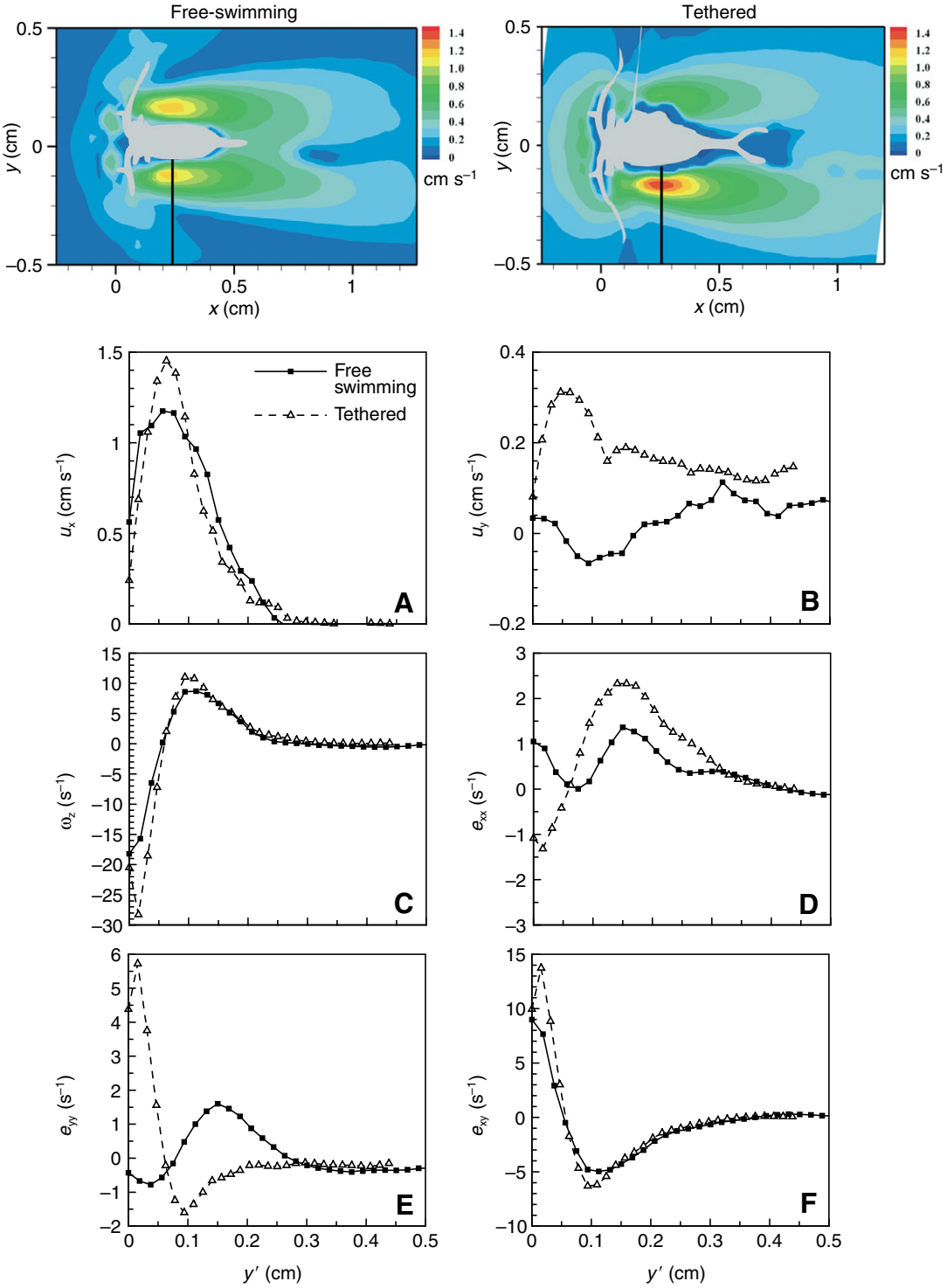

Fig. 8. Exemplary profiles along the highlighted direction for the free-swimming and tethered *Euchaeta antarctica*. The profile direction in the dorso-ventral view is oriented at 90° relative to the center axis of the organism and passes through the location of maximum velocity. Profiles correspond to (A) u_x, (B) u_y, (C) ω_z, (D) e_{xx}, (E) e_{yy}, and (F) e_{xy}. y' is zero at the location of the organism body rather than at the organism center axis.

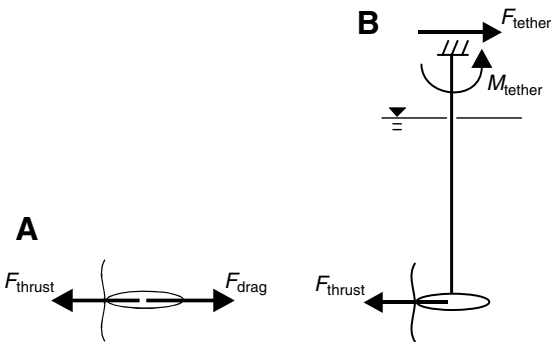

Fig. 9. Free body diagram for the (A) free swimming and (B) tethered copepods. M_{tether}, moment on the tether support.

As noted for the tropical congener of this copepod (Lenz and Yen, 1993), the intensity of the anterior flow field declines toward the distal tips of *E. antarctica*. Hence, the mechanoreceptive sensors extend beyond the induced flow field, which enables sensing of an approaching predator. In front of the antennules, the anterior feeding current velocity has a double maximum where the longest mechanosensory hairs are located (Fig. 3A) (see also Yen and Nicoll, 1990). The structure of the feeding current appears to be optimized for detecting prey escapes (closest to mechanosensors) and for aggregating prey where they can be captured (i.e. within capture range of this carnivorous copepod).

With regard to the mechanoreceptive signal generated by *E. antarctica*, Fig. 8D–F suggests that e_{xy} is the largest component of the strain rate in the induced flow field. Shear strain rates greater than 2 s^{-1} (maximum of around 10 s^{-1}) surround the locomotory appendage region, which demonstrates the intensity of the copepodid-generated flow disturbance. The 0.5 s^{-1} contour of e_{xy} for the free-swimming case (Fig. 11A,C), which is a likely threshold to induce an escape response (Fields

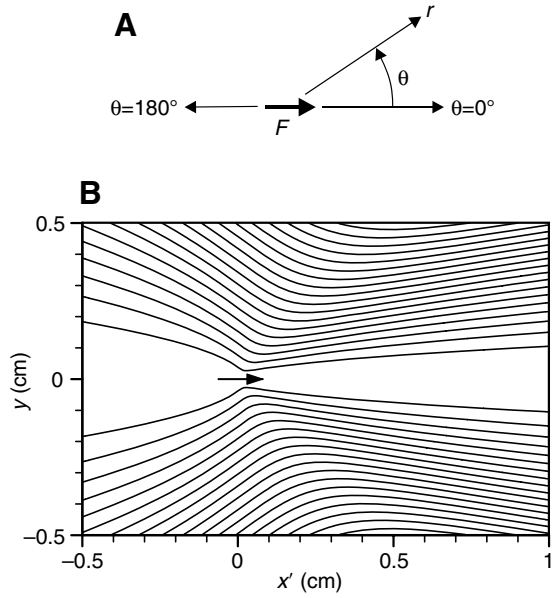

Fig. 10. (A) Coordinate system and (B) streamline pattern for the theoretical solution of a force at the origin pointed to the right. C=0.4 for the streamlines shown. x' is zero at the location of the tether, rather than at the head of the organism.

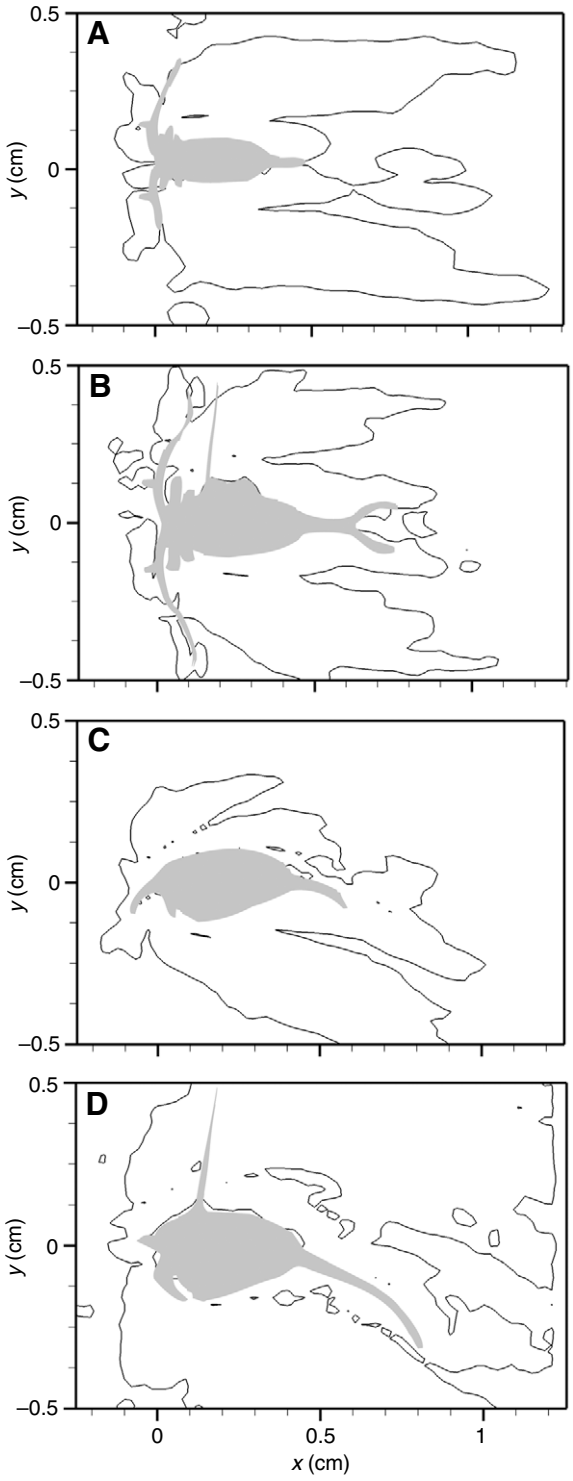

Fig. 11. The 0.5 s^{-1} contour of strain rate (e_{xy}) for (A,C) a free-swimming, and (B,D) a tethered *Euchaeta antarctica*. The 0.5 s^{-1} contour is shown as a representative value that has been observed to induce escape response in copepods (Fields and Yen, 1997; Kiørboe et al., 1999).

and Yen, 1997; Kiørboe et al., 1999), provides a measure of the spatial extent of the signal for other mechanoreceptive predators. The area in the dorso-ventral view surrounded by the 0.5 s^{-1} contour is 11 times the area of the exoskeletal form. Hence, mechanoreceptive predators will perceive a much more spatially extended signal than the body size. The 0.5 s^{-1} contour of e_{xy} for the tethered specimen in the side view (Fig. 11D) shows that the extent of the strain rate field is much greater in the tethered case (the contour extends beyond the boundaries of the measured field). Thus, the spatial extent of the mechanoreceptive signal would be overestimated with these data for the tethered specimen. Alternatively, the spatial extent of the 0.5 s^{-1} contour for the tethered copepodid in the dorso-ventral view (Fig. 11B) is similar or slightly reduced compared to the free swimming case (Fig. 11A). The differences in the strain rate fields for the free-swimming and tethered copepodid field demonstrate the subtle influence of altering the spatial distribution of the flow field due to the physical presence of the tether (described above) and perhaps due to the behavioral changes of the organism. This comparison highlights the importance of using a free-swimming flow field when making sensory ecology conclusions.

The authors wish to thank Xiaodong Tian, Oahn Lu and Jen Sehn for assistance with data analysis. Financial support was provided by NSF OPP-0324539 and a NSF-IGERT fellowship awarded to K.B.C.

References

Alcaraz, M., Paffenhöfer, G. A. and Strickler, J. R. (1980). Catching the algae: a first account of visual observations on the filter feeding calanoids. In *Evolution and Ecology of Zooplankton Communities: Special Symposium of the American Society of Limnology and Oceanography*. Vol. 3 (ed. W. C. Kerfoot), pp. 241-248. Hanover: University Press of New England.

Bundy, M. H. and Paffenhöfer, G. A. (1996). Analysis of flow fields associated with freely swimming calanoid copepods. *Mar. Ecol. Prog. Ser.* **133**, 99-113.

Cohen, J. H. and Forward, R. B., Jr (2002). Spectral sensitivity of vertically migrating marine copepods. *Biol. Bull.* **203**, 307-314.

Coombs, S., Janssen, J. and Webb, J. C. (1988). Diversity of lateral line systems: evolutionary and functional considerations. In *Sensory Biology of Aquatic Animals* (ed. J. Atema, R. Fay, A. N. Popper and W. N. Tavolga), pp. 553-594. New York: Springer Verlag.

Drucker, E. G. and Lauder, G. V. (2002). Experimental hydrodynamics of fish locomotion: functional insights from wake visualization. *Integr. Comp. Biol.* **42**, 243-257.

Emlet, R. B. (1990). Flow fields around ciliated larvae: effects of natural and artificial tethers. *Mar. Ecol. Prog. Ser.* **63**, 211-225.

Fields, D. M. and Yen, J. (1993). Outer limits and inner structure: the 3-dimensional flow field of *Pleuromamma xiphias* (Calanoida: Metridinidae). *Bull. Mar. Sci.* **53**, 84-95.

Fields, D. M. and Yen, J. (1997). The escape behavior of marine copepods in response to a quantifiable fluid mechanical disturbance. *J. Plankton Res.* **19**, 1289-1304.

Gallager, S. M. (1988). Visual observations of particle manipulations during feeding in larvae of a bivalve mollusk. *Bull. Mar. Sci.* **43**, 344-365.

Gallager, S. M. (1993). Hydrodynamic disturbances produced by small zooplankton: a case study for the veliger larva of a bivalve mollusk. *J. Plankton Res.* **15**, 1277-1296.

Hwang, J., Turner, J. T., Costello, J. H., Coughlin, D. J. and Strickler, J. R. (1993). A cinematographic comparison of behavior by the calanoid copepod *Centropages hamatus* Lilljeborg: tethered versus free-swimming animals. *J. Exp. Mar. Biol. Ecol.* **167**, 277-288.

Jiang, H. S., Meneveau, C. and Osborn, T. R. (1999). Numerical study of the feeding current around a copepod. *J. Plankton Res.* **21**, 1391-1421.

Jiang, H. S., Meneveau, C. and Osborn, T. R. (2002). The flow field around a freely swimming copepod in steady motion. Part II: Numerical simulation. *J. Plankton Res.* **24**, 191-213.

Kiørboe, T., Saiz, E. and Visser, A. W. (1999). Hydrodynamic signal perception in the copepod *Acartia tonsa*. *Mar. Ecol. Prog. Ser.* **179**, 97-111.

Koehl, M. A. R. and Strickler, J. R. (1981). Copepod feeding currents: food capture at low Reynolds number. *Limnol. Oceanogr.* **26**, 1062-1073.

Landau, L. (1944). A new exact solution of Navier-Stokes equations. *Dokl. Akad. Nauk SSSR* **43**, 286-288.

Lenz, P. H. and Yen, J. (1993). Distal setal mechanoreceptors of the first antennae of marine copepods. *Bull. Mar. Res.* **53**, 170-179.

Malkiel, E., Sheng, J., Katz, J. and Strickler, J. R. (2003). The three-dimensional flow field generated by a feeding calanoid copepod measured using digital holography. *J. Exp. Biol.* **206**, 3657-3666.

Naudascher, E. (1965). Flow in the wake of self-propelled bodies and related sources of turbulence. *J. Fluid Mech.* **22**, 625-656.

Nogueira, J., Lecuona, A. and Rodriquez, P. A. (1997). Data validation, false vectors correction and derived magnitudes calculation on PIV data. *Meas. Sci. Technol.* **8**, 1493-1501.

Raffel, M., Willert, C. and Kompenhans, J. (1998). *Particle Image Velocimetry – A Practical Guide*. New York: Springer-Verlag.

Schlichting, H. and Gersten, K. (2000). *Boundary Layer Theory*. Berlin: Springer-Verlag.

Sherman, F. S. (1990). *Viscous Flow*. New York: McGraw-Hill.

Sirviente, A. I. and Patel, V. C. (2000). Wake of a self-propelled body. Part 1. Momentumless wake. *AIAA J.* **38**, 613-619.

Squire, H. B. (1951). The round laminar jet. *Quart. J. Mech. Appl. Math.* **4**, 321-329.

Stamhuis, E. J., Videler, J. J., van Duren, L. A. and Muller, U. K. (2002). Applying digital particle image velocimetry to animal-generated flows: traps, hurdles and cures in mapping steady and unsteady flow in *Re* regimes between 10^{-2} and 10^{5}. *Exp. Fluids* **33**, 801-813.

Stearns, D. E. and Forward, R. B., Jr (1984). Photosensitivity of the calanoid copepod *Acartia tonsa*. *Mar. Biol.* **82**, 85-89.

Strickler, J. R. (1977). Observation of swimming performances of planktonic copepods. *Limnol. Oceanogr.* **22**, 165-170.

Strickler, J. R. (1982). Calanoid copepods, feeding currents, and the role of gravity. *Science* **218**, 158-160.

Tiselius, P. and Jonsson, P. R. (1990). Foraging behavior of six calanoid copepods: observations and hydrodynamic analysis. *Mar. Ecol. Prog. Ser.* **66**, 23-33.

van Duren, L. A. and Videler, J. J. (2003). Escape from viscosity: the kinematics and hydrodynamics of copepod foraging and escape swimming. *J. Exp. Biol.* **206**, 269-279.

van Duren, L. A., Stamhuis, E. J. and Videler, J. J. (1998). Reading the copepod personal ads: Increasing encounter probability with hydromechanical signals. *Philos. Trans. R. Soc. Lond. B* **353**, 691-700.

van Duren, L. A., Stamhuis, E. J. and Videler, J. J. (2003). Copepod feeding currents: flow patterns, filtration rates and energetics. *J. Exp. Biol.* **206**, 255-267.

Westerweel, J. (1994). Efficient detection of spurious vectors in particle image velocimetry data. *Exp. Fluids* **16**, 236-247.

Westerweel, J. (1997). Fundamentals of digital particle image velocimetry. *Meas. Sci. Technol.* **8**, 1379-1392.

Woodson, C. B., Webster, D. R., Weissburg, M. J. and Yen, J. (2005). Response of copepods to physical gradients associated with structure in the ocean. *Limnol. Oceanogr.* **50**, 1552-1564.

Yen, J. and Fields, D. M. (1992). Escape responses of *Acartia hudsonica* (copepoda) nauplii from the flow field of *Temora longicornis* (copepoda). *Arch. Hydrobiol. Beih. Ergebn. Limnol.* **36**, 123-134.

Yen, J. and Nicoll, N. T. (1990). Setal array on the 1st antennae of a carnivorous marine copepod, *Euchaeta norvegica*. *J. Crust. Biol.* **10**, 218-224.

Yen, J. and Strickler, J. R. (1996). Advertisement and concealment in the plankton: what makes a copepod hydrodynamically conspicuous? *Invertebr. Biol.* **115**, 191-205.

Yen, J., Sanderson, B., Strickler, J. R. and Okubo, A. (1991). Feeding currents and energy dissipation by *Euchaeta rimana,* a subtropical pelagic copepod. *Limnol. Oceanogr.* **36**, 362-369.

Yen, J., Weissburg, M. J. and Doall, M. H. (1998). The fluid physics of signal perception by mate-tracking copepods. *Philos. Trans. R. Soc. Lond. B* **353**, 787-804.